Supplemental Material

Journal of Hydrometeorology

Evaluation of Noah-MP Snow Simulation across Site Conditions in the Western United States

https://doi.org/10.1175/JHM-D-23-0211.1

Supplemental Information

Contents of this file

Text S1: Eco-regions

We assigned each station to an eco-region based on the Commission for Environmental Cooperation (CEC) Terrestrial Ecoregions Level III classification (Wilken et al. 2011). These eco-regions are defined by both data and expert opinion using a holistic range of diagnostic criteria including soils, physiography, water bodies, major vegetation type, land use and other human influences, and climates. For illustration purposes in this study, certain nearby eco-regions were combined because model behavior was similar. North Cascades, Klamath Mountains, and Cascades were joined to become “Cascades”; Columbia Mountains/Northern Rockies, Idaho Batholith, and Middle Rockies were joined to become “Northern Rockies”; and Northern Basin and Range and Central Basin and Range were joined to become “Basin and Range”. Four regions contained only a single station located close to the region boundary; these stations were added to the most nearby region. A single station in the Colorado Plateau was added to Wasatch and Unita Mountains region; a single station in Wyoming Basin was joined with the Northern Rockies; a single station in the Coast Range was added to the Cascades; and a single station in the Snake River Basin was joined with the Idaho Batholith (Northern Rockies).

Text S2: SNOTEL Meteorological Records QA/QC

Daily precipitation and SWE values were taken from the bias-corrected quality-controlled data product published by Yan et al. (2018). These data have undergone a three-stage quality control (QC) filter to eliminate outliers and erroneous or inconsistent observations. The quality-controlled precipitation data is then corrected for potential under-catch of snowfall, which has been widely observed at SNOTEL stations due to wind processes and wetting loss on collector walls (e.g., Livneh et al. 2014; Serreze et al. 1999; Sun et al. 2019).

While the Yan et al. (2018) data product also includes quality-controlled and bias-corrected daily temperature records, we chose to instead use hourly temperature data for this study because the Noah-MP model is run at an hourly time step. So, hourly temperature data was downloaded in raw form from the NRCS web portal for over 800 SNOTEL stations. A two-stage QC filter was applied to these records. First, outliers were removed based on global minimum/maximum thresholds of +39 °C and -50 °C (Livneh et al. 2014). Second, following the statistics-based approach used by Serreze et al. (1999) and Yan et al. (2018), values lying outside of +/- three standard deviations from the daily average were removed as outliers. We chose to compute these statistics at the daily level rather than hourly in order to include more data points for each day of the water year.

Only stations with less than 5% missing quality-controlled hourly temperature and daily precipitation and no missing daily SWE over the study period of record (water years 2007-2019) were selected for further study. Data gaps were then filled in order to generate complete records for model input. This process was applied to hourly temperature data over three steps. First, short-term gaps (identified as 5 continuous hours or less) were completed with linear interpolation, following the method in Sun et al. (2019). Second, long-term gaps (identified as 6 continuous hours or longer) were filled in by regressing each station data on nearby stations that have data available during those missing time steps. For this, linear regressions were fitted between each station data and the 10 closest stations that have greater than half of usable hourly temperature records. The neighboring station with the highest R^2 value is used first to predict the missing temperature data. Remaining missing data is filled in by using the station with the next highest R^2 value, and so on. Third, if data is still missing (in this case, an average of 9 hours in about a quarter of the stations), the remaining gaps are filled in with the station's climatological mean for that hour of the water year. Only one of the selected stations had gaps in daily precipitation data – this was filled in by regressing the station's precipitation records with the nearest 5 stations and selecting the one with the highest R^2 value to predict the missing values.

A warm bias at cold temperatures has been noted at SNOTEL stations in numerous studies; this has been attributed to erroneous conversion from voltages to degrees C (Harms et al. 2016; Currier et al. 2017; Oyler et al. 2015). So, we applied a linear equation that was developed by Harms et al., 2017 and subsequently applied in several studies (e.g., Currier et al. 2017; Sun et al. 2019) to correct this error:

$$T_{corr} = 1.03 * T_{sntl} - 0.9 \qquad (1)$$

where T_{sntl} is the SNOTEL raw temperature observation (°C).

Text S3: AORC Forcings

The Analysis of Record for Calibration (AORC) forcings include: precipitation, temperature, specific humidity, terrain-level pressure, downward longwave and shortwave radiation, and west-east and south-north wind components (AORC version 1.1). The dataset is constructed from over a dozen individual datasets, including: North American Regional Reanalysis (NARR), NLDAS2, and National Centers for Environmental Prediction (NCEP) Global Data Assimilation System (GDAS); and was bias-corrected by gauge-based climatological datasets including PRISM, Livneh et al. (2015), Vose et al. (2014), and Hill et al. (2015). Compared to quality-controlled bias-corrected SNOTEL observations, AORC winter precipitation is on average 10.6% less, with most (82%) stations showing less precipitation in AORC than in the SNOTEL record (Figure S1a,c). AORC winter temperatures are also on average lower than SNOTEL (average of -0.2°C), but the differences are more heterogenous across stations (Figure S1b,d).

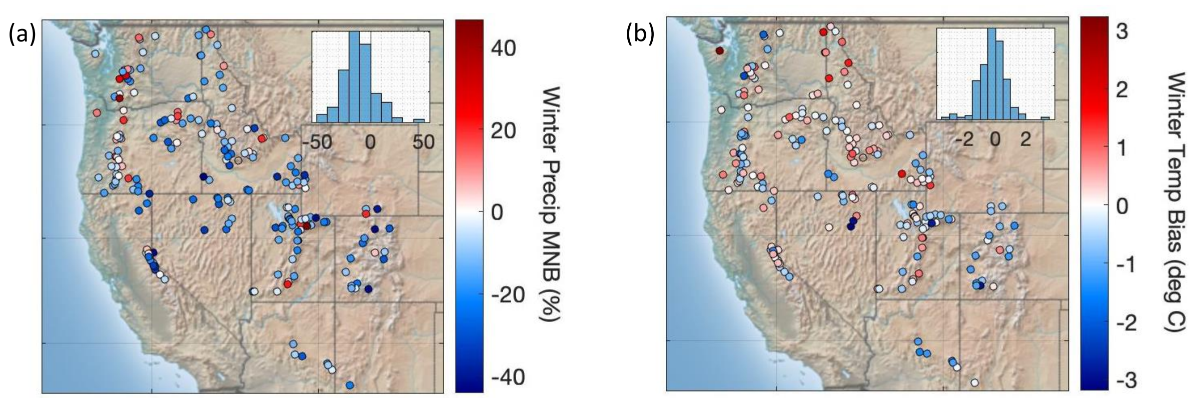

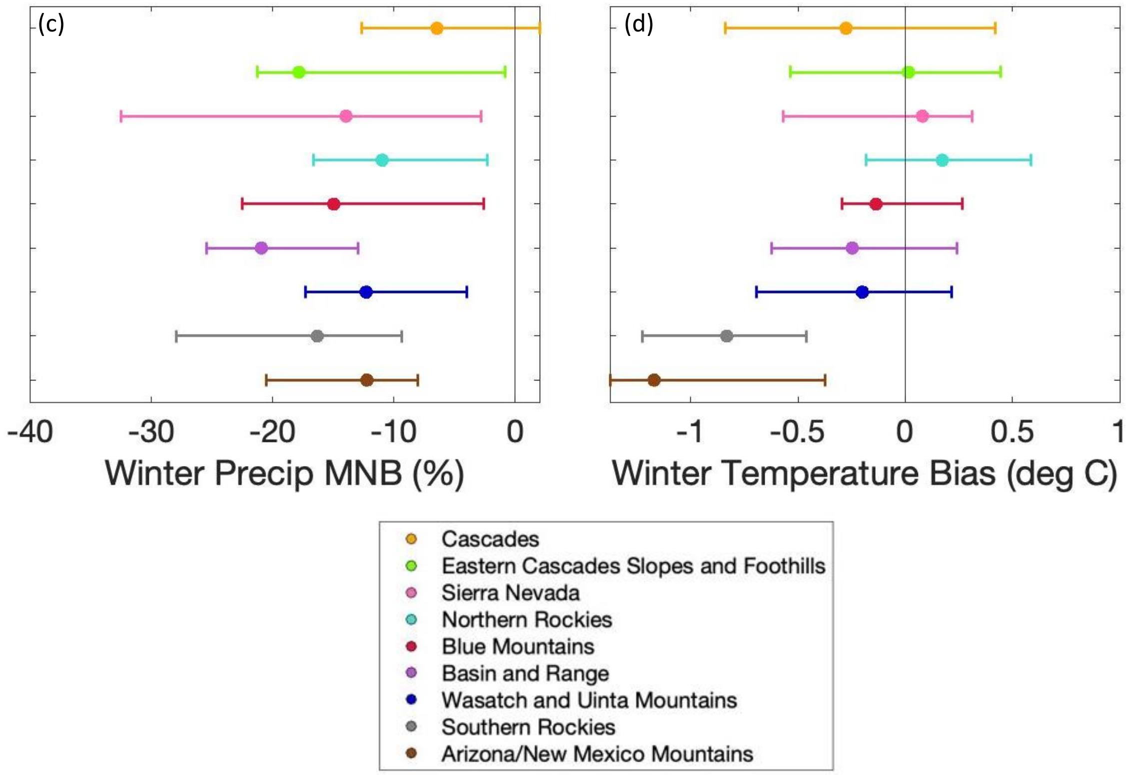

Figure S1. Bias between AORC and SNOTEL winter (Nov-March) precipitation (a) and winter temperature (b) across 199 sites in WYs 2007-2019. Bias in precipitation is computed as the mean normalized bias, and bias in air temperature is computed as the difference. These sites are classified into eco-regions, for which the bias for winter precipitation is shown in (c), and for winter temperature in (d). Circles mark the median of the subgroup, and the width of the line marks the interquartile range.

Text S4: Physics processes in alternative model experiments

Precip2.2 and Precip0 test alternative options for precipitation partitioning into snow and rain, and should primarily impact snow accumulation by changing input snowfall (Figure S2). The base case option for snow/rain partitioning defines a prescribed linear snowfall fraction when air temperature is between 0.5 and 2.5 °C (Jordan 1991). Precip2.2 instead sets a fixed threshold for snow at 2.2 °C, while Precip0 uses 0 °C. Note that recent studies have explored precipitation partitioning with wet-bulb temperature rather than air temperature (Wang et al. 2019, Letcher et al. 2022) and have found that this improves model performance; the Wang et al. 2019 wet-bulb temperature-based precipitation partitioning scheme is now included in the latest version of Noah-MP (v5, He et al. 2023).

Alb tests the alternative option for snow surface albedo, impacting snowmelt by changing net radiation (Figure S2). The base case uses BATS (Biosphere-Atmosphere Transfer Scheme, Dickinson et al. 1986, Yang et al. 1997), which calculates snow albedo for direct and diffuse radiation in visible and near-infrared broadband (Niu et al. 2011). The alternative uses CLASS (Canadian Land Surface Scheme), which computes snow albedo from fresh snow albedo and snow age. BATS with default parametrization has been shown to overestimate snow albedo (Niu et al. 2011; Abolafia-Rosenzweig et al. 2022).

ResisDrag and ResisEvap test alternative options for the surface layer drag coefficient and surface resistance to evaporation/sublimation processes, impacting snowmelt through the computation of surface energy fluxes (Figure S2). The base case sets the surface resistance to evaporation/sublimation as a constant parameter (rsurf,snow = 50s/m) if the surface is snowy. The alternative used in ResisEvap instead employs the Sakaguchi and Zeng (2009) algorithm for surface resistance for all grid cells regardless of snowiness. This algorithm, defined for NCAR's CLM3.5, describes a surface resistance that explicitly represents the effects of plant litter cover, under-canopy stability, and turbulent resistance; as such, the surface resistance is often above 50s/m but varies by season, water content, and vegetation (Sakaguchi and Zeng 2009). This surface resistance algorithm has been found to decrease modeled latent heat flux in the Western US, but with no significant changes to snow depth (Sakaguchi and Zeng 2009).

The surface layer drag coefficient is determined either by the Monin-Obukhov similarity theory in the base case, or by the original Noah approach (Chen 1997) in ResisDrag. The Chen (1997) approach has been observed to produce a lower surface drag coefficient (e.g., Zhang et al. 2014), which would lead to a higher aerodynamic resistance and lower values for sensible and latent heat fluxes in ResisDrag.

TempSolv and TempLB use alternative options for the lower boundary condition of soil temperature and snow/soil temperature in the model's soil heat flux calculation, respectively, and are expected to impact melt processes via the dissipation of energy in the soil (Figure S2). The lower soil temperature boundary condition is set by a read-from-file parameter in the base case. TempLB instead prescribes zero heat flux from the bottom of the soil column. The snow/soil temperature time scheme is a solver option rather than a physics option: in the base case, fractional snow cover is considered in the semi-implicit solution to the thermal diffusion equation, whereas it is not considered in the alternative (TempSolv). The thermal diffusion equation affects upper soil and lower snow layer temperatures.

DynVeg, the experiment for the dynamic vegetation option, affects both accumulation and melt processes (Figure S2). In the base case, the dynamic vegetation module is turned off; instead, parameters like leaf area index (LAI) and maximum vegetation fraction are based on ground- and satellite- observations. The dynamic vegetation module models prognostic vegetation growth (Dickinson et al. 1998), by combining Ball-Berry photosynthesis-based stomatal resistance with dynamic vegetation and allocating carbon to different parts of vegetation. Vegetation can influence snow processes by: intercepting snow, changing total albedo, changing heat flux with soil temperature, or re-emitting radiation downwards (Park and Park 2016). Based on how the dynamic vegetation module changes the parameters that affect these processes (for example, a larger LAI would intercept more snow), the difference in snow simulation between DynVeg and the base case varies by vegetation type.

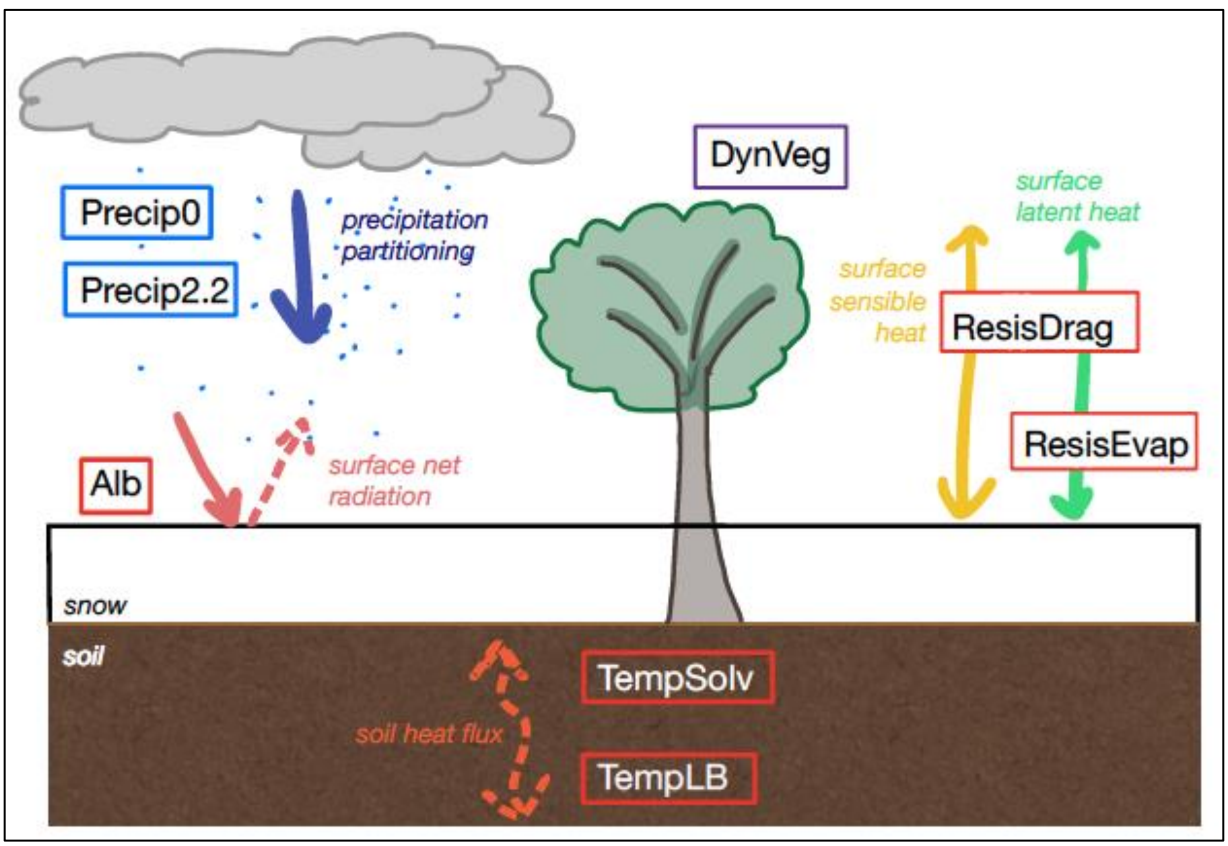

Figure S2. Schematic of a snow model with relevant model physics processes. Experiments tested in this study are boxed and placed near the relevant physics processes. Those labeled with a blue box are ones that primarily impact snow accumulation processes; those with a red box should impact snowmelt processes; and those with a purple box should impact both.

	NOAA NWM 2.0 options		WRF-Hydro recommended options	
Option	**Value**	**Definition**	**Value**	**Definition**
DYNAMIC_VEG_OPTION: options for dynamic vegetation	4	off (use table LAI; use maximum vegetation fraction)	4	off (use table LAI; use maximum vegetation fraction)
CANOPY_STOMATAL_RESISTANCE_OPTION: options for canopy stomatal resistance	1	Ball-Berry	1	Ball-Berry
BTR_OPTION: option for soil moisture factor for stomatal resistance	1	Noah (soil moisture)	1	Noah (soil moisture)
RUNOFF_OPTION: options for runoff and groundwater	3	Original surface and subsurface runoff (free drainage)	3	Original surface and subsurface runoff (free drainage)
SURFACE_DRAG_OPTION: options for surface layer drag coeff (CH & CM)	1	M-O	1	M-O
FROZEN_SOIL_OPTION: options for frozen soil permeability	1	Linear effects; more permeable (Niu and Yang 2006)	1	Linear effects; more permeable (Niu and Yang 2006)
SUPERCOOLED_WATER_OPTION: options for supercooled liquid water (or ice fraction)	1	No iteration (Niu and Yang 2006)	1	No iteration (Niu and Yang 2006)
RADIATIVE_TRANSFER_OPTION: options for radiation transfer	3	Two-stream applied to vegetated fraction (gap = 1-FVEG)	3	Two-stream applied to vegetated fraction (gap = 1-FVEG)
SNOW_ALBEDO_OPTION: option for ground snow surface albedo	1	BATS	2	CLASS
PCP_PARTITION_OPTION: options for partitioning precipitation into rainfall & snowfall	1	Jordan (1991)	1	Jordan (1991)
TBOT_OPTION: options for lower boundary condition of soil temperature	2	TBOT at ZBOT (8m) read from a file (original Noah)	2	TBOT at ZBOT (8m) read from a file (original Noah)
TEMP_TIME_SCHEME_OPTION: options for snow/soil temperature time scheme (only layer 1)	3	Semi-implicit; flux top boundary condition, but FSNO for TS calculation (generally improves snow; v 3.7)	1	Semi-implicit; flux top boundary condition
GLACIER_OPTION: options for glacier treatment	2	Ice treatment more like original Noah (slab)	2	Ice treatment more like original Noah (slab)
SURFACE_RESISTANCE_OPTION: options for surface resistent to evaporation/sublimation	4	Sakaguchi and Zeng (2009) for non-snow; rsurf=rsurf_snow for snow (set in MPTABLE); AD v.3.8	1	Sakaguchi and Zeng (2009)

Table S1. List of physics options in Noah-MP, with indicators of usage with WRF-Hydro/NWM. Summarized from Gochis et al. (2018).

							Percent by vegetation type				
Region	**Number of stations**	**Elevation (m)**	**Winter PPT (mm)**	**Winter Temp (deg C)**	**Accumulated SWE (mm)**	**DOWY Peak SWE (day)**	*Barren or Sparsely Vegetated*	*Evergreen Needleleaf*	*Grassland*	*Shrubland*	*Deciduous Broadleaf Forest*
Cascades	39	1282	1233	-0.12	796	169 (Mar 19)	3%	34%	53%	8%	3%
Eastern Cascades Slopes and Foothills	11	1761	549	-1.04	480	157 (Mar 7)	9%	9%	55%	27%	0%
Sierra Nevada	12	2225	886	-0.58	734	168 (Mar 18)	33%	17%	17%	33%	0%
Northern Rockies	42	1975	634	-4.15	624	183 (Apr 2)	2%	21%	50%	24%	2%
Blue Mountains	17	1669	597	-1.81	533	170 (Mar 20)	6%	24%	65%	6%	0%
Basin and Range	24	2247	461	-1.82	480	174 (Mar 24)	29%	17%	21%	29%	4%
Wasatch and Uinta Mountains	30	2563	449	-3.76	512	180 (Mar 30)	0%	10%	60%	10%	20%
Southern Rockies	17	2997	465	-5.25	562	189 (Apr 8)	6%	18%	76%	0%	0%
Arizona/New Mexico Mountains	7	2500	375	1.75	264	135 (Feb 13)	14%	29%	43%	14%	0%

Table S2. Mean characteristics of SNOTEL stations used in study, as grouped by eco-region. Climate and SWE variables are observed historical means for WYs 2007 to 2019. Winter is defined as months Nov-March. Winter precipitation (PPT) is the sum over that period, whereas winter temperature is the average over that period. Accumulated SWE is the sum of positive daily changes in SWE for the entire water year.

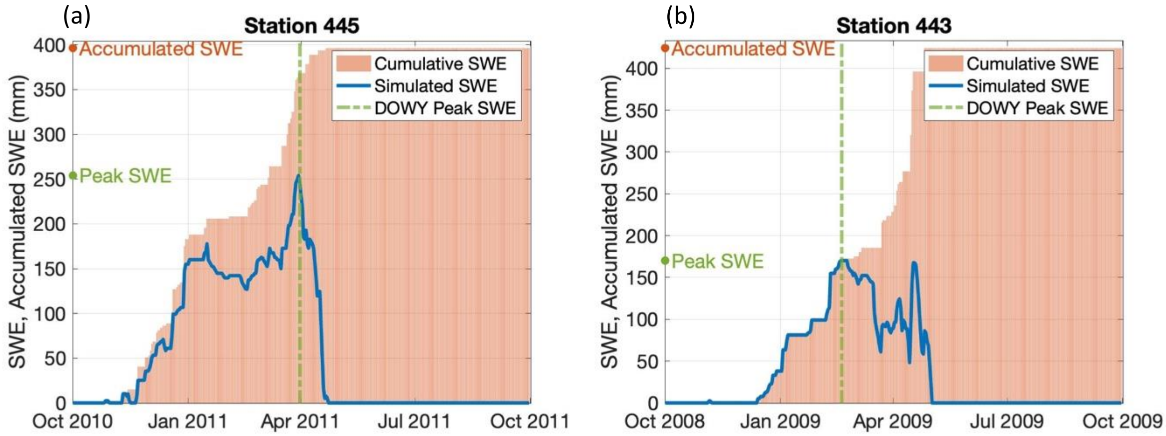

Figure S3. Illustrations of observed SWE from SNOTEL station-years when a single-day snow metric like peak SWE significantly underestimates the totality of SWE being produced over the course of the water year. DOWY for peak SWE is indicated with a vertical green line, and peak SWE depth is indicated with a blue dot on the y-axis. Cumulative accumulated snowmelt is illustrated with orange bars and yearly accumulated SWE is marked with an orange dot on the y-axis. (a) WY 2011 at SNOTEL station 445 shows a case of pre-peak SWE melt. (b). WY 2009 at SNOTEL station 443 shows a case of post-peak SWE accumulation.

Text S5: Removing propagated uncertainty from daily changes in SWE

The daily accumulation and melt rates are computed as the average positive or negative changes in daily SWE over the water year. Because we are comparing modeled results to observed measurements, we have to acknowledge differences in precision between the two. The SNOTEL snow pillow's precision is 0.254 mm, which we take as the detection limit. The propagated uncertainty from this single-day detection limit into values of daily changes (i.e., $SWE_{n+1} - SWE_n$) is computed as:

$$s_{\Delta SWE} = \sqrt{\left(s_{SWE_n+1}\right)^2 + \left(s_{SWE_n}\right)^2} \qquad (2)$$

based on the rules of propagating uncertainty when adding or subtracting measurements (i.e., Kirchner, J. 2001). Here, we are replacing the typical standard deviation with the daily detection limit when describing the original measurement uncertainty. So, with a 2.54 mm uncertainty in the original measurement, the propagated uncertainty is 3.58 mm. Daily SWE changes below this value were set to zero in both simulated and observed records to maintain consistency, because the in situ sensor may not be capable of deriving differences below this level.

Text S1: Application of Kolmogorov-Smirnov (KS) test to evaluate model sensitivity

We applied the Kolmogorov-Smirnov (KS) test to evaluate model sensitivity. This test has been utilized to assess model sensitivity for numerous hydrology model studies (e.g., He et al. 2011; Sun et al. 2019). In general, this statistical test is used to decide if a sample comes from a population with a specific distribution. Applied as a two-sample test, KS can be used to test whether two underlying probability distributions differ. In this case, the KS statistic is computed as the maximum vertical distance between the two empirical distribution functions:

$$\mathrm{KS} = \sup_{x}\left|\mathrm{F}_{1,n}(x) - \mathrm{F}_{2,m}(x)\right| \qquad (3)$$

where sup is the supremum function, and $\mathrm{F}_{1,n}$ and $\mathrm{F}_{2,m}$ are the empirical distribution functions of the first and second sample (Chakravarti et al. 1997).

In this study, for each station and for each snow metric, we apply a two-sample KS test with the yearly snow metric values from the base case and from the experiment as the two sets of inputs. For example, **Error! Reference source not found.** illustrates how the KS statistic is computed at Station 302 for the accumulated SWE metric, between the base case and Precip0. The empirical distributions include all yearly accumulated SWE metrics for the base case at that station in blue, and for the Precip0 experiment in orange. The maximum distance between the curves is indicated with the black arrow, and equals the KS statistic. KS values range from 0 to 1, with higher values indicating greater sensitivities. We used a minimum KS threshold value of 0.5 to identify sensitivity because it yields statistically significant results at p-value < 0.1. So, stations with a KS statistic equal to or greater than 0.5 were considered sensitive to that alternative model configuration for that snow metric.

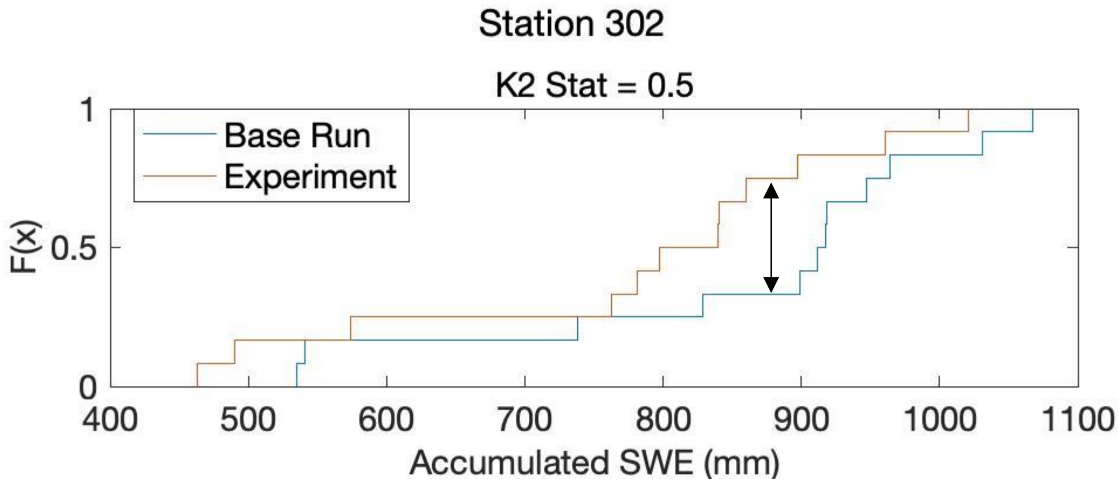

Figure S4. Example of computation of KS statistic, on the accumulated SWE metric and between the base case and Precip0 experiment at Station 302. The black arrow indicates the value of the KS statistic.

Text S2: Model performance across model configurations

Noah-MP predictions tend to overestimate observed accumulated SWE across most sites and for all model configurations except for the Precip0 and AORC experiments (Figure S5a). All model configurations but the AORC experiment shows a model underestimation in storm rate, and a model overestimation in timing of peak SWE (Figure S5b,d). The AORC experiment, and to a lesser degree, the Precip0 experiment, shows a high FNR for accumulation days (median of 50% and 15%, respectively), whereas the rest of the experiments have FNRs of less than 10% (Figure S5e). The model consistently underestimates daily average melt rate across all model configurations (Figure S5f). AORC and Precip0 show the highest FNR for melt days, but the FNR for melt days is higher across all experiments (between 35% and 54%) (Figure S5f), suggesting that the model fails at simulating observed melt events more frequently than it does for accumulation events.

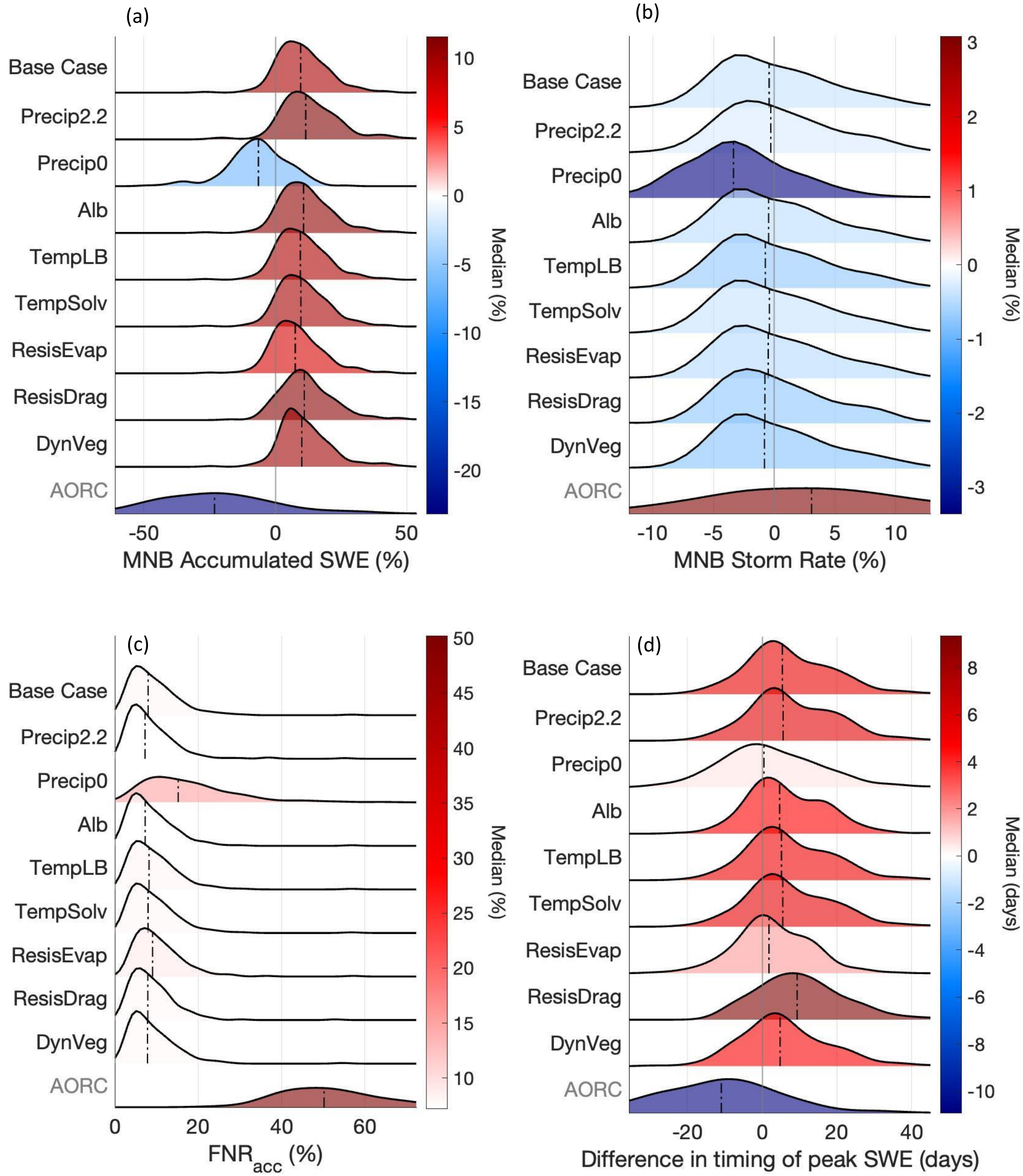
(a)
Base Case
Precip2.2
Precip0
Alb
TempLB
TempSolv
ResisEvap
ResisDrag
DynVeg
AORC
-50
0
50
MNB Accumulated SWE (%)
Median (%)
(b)
MNB Storm Rate (%)
Median (%)
(c)
FNR$_{acc}$ (%)
Median (%)
(d)
Difference in timing of peak SWE (days)
Median (days)

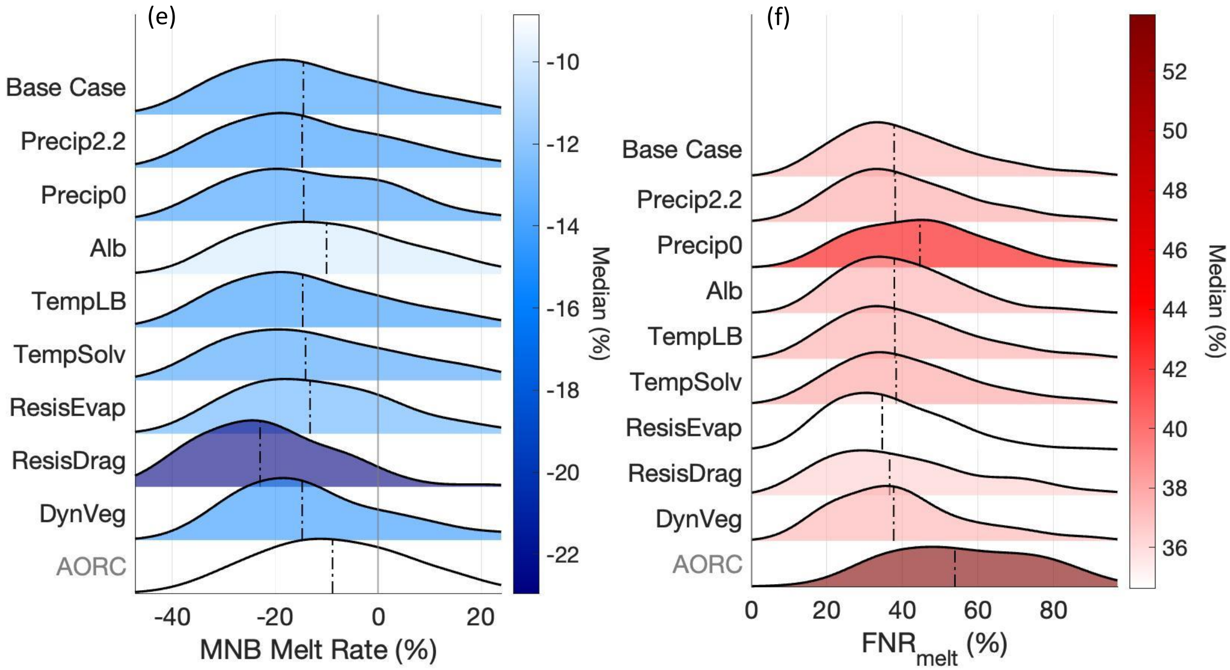

Figure S5. Distributions of model performance across SNOTEL stations and nine model configurations for four snow metrics. (a) mean normalized bias (MNB) of accumulated SWE, (b) MNB of storm rate, (c) average false negative rate (FNR) for accumulation days, (d) difference in timing of peak SWE, (e) MNB of daily melt rate, and (f) average FNR for melt days. Bias metrics are computed for each station-year with reference to the observed SNOTEL records, and then averaged for each station over the time period. The color of the distribution and dashed horizontal line corresponds to the median metric value for each model configuration. A blue (red) color indicates the model configuration produces a lower (higher) median metric value than the observation.

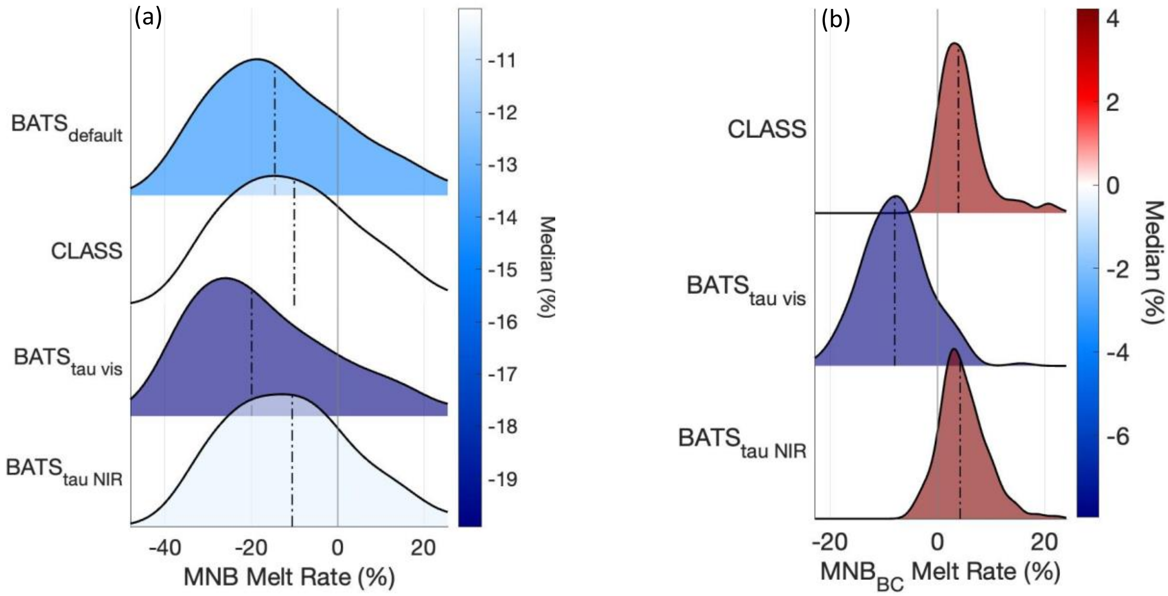

Figure S6. (a) Distributions of model performance across SNOTEL stations and four model configurations related to snow albedo, as described by mean normalized bias (MNB) of melt rate. BATS$_{default}$ refers to the Base Case (Table 2 in main text) with all default parameters. CLASS refers to the Alb experiment, which utilizes the CLASS albedo scheme. BATS$_{tau_vis}$ and BATS$_{tau_NIR}$ refer to experiments with the BATS albedo model but with the snow age parameter τ_0 adjusted to values optimized in Abolafia-Rosenzweig et al. (2022). A blue (red) color indicates the model configuration produces a lower (higher) median metric value than the observation. (b) Distributions of changes in the MNB of melt rate relative to the base case across SNOTEL stations and the three alternative snow albedo-related experiments. Bias metrics (MNB$_{BC}$, **Error! Reference source not found.**) are computed for each station-year with reference to the base case, and then averaged for each station over the time period. The distribution color and the dashed horizontal line correspond to the median bias value for each experiment. A red (blue) color indicates the model configuration produces a higher (lower) median value than the base case.

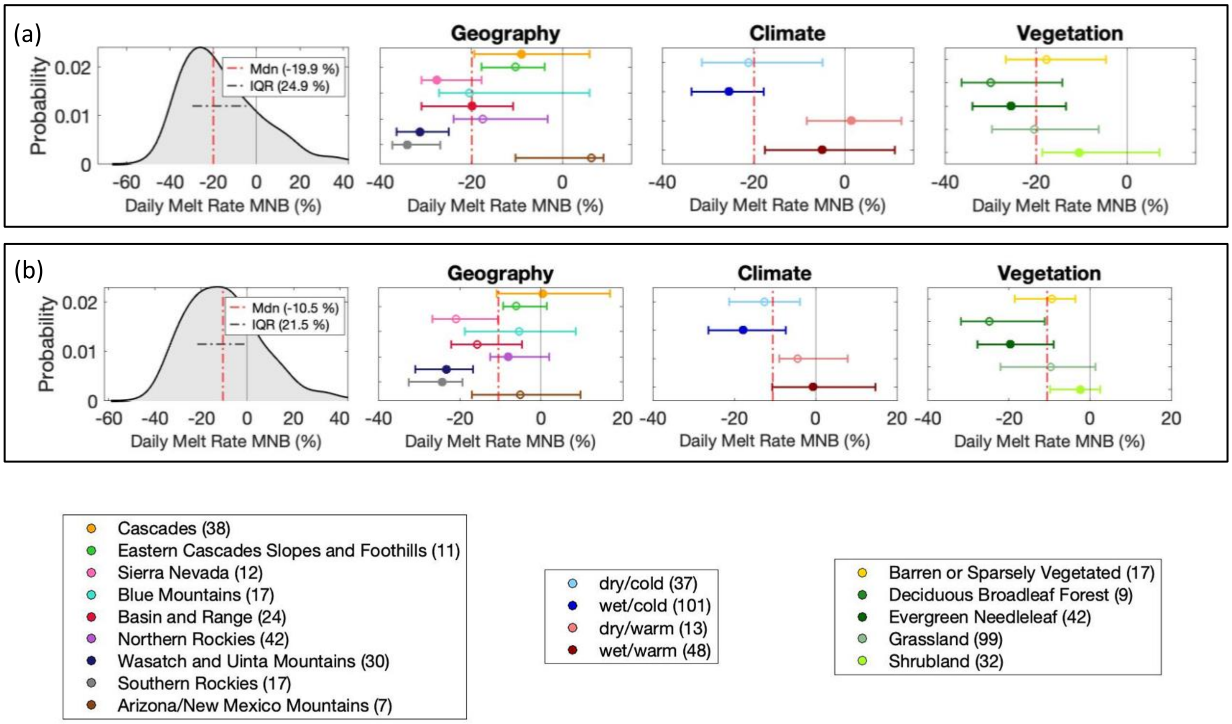

Figure S7. Model performance (MNB in daily melt rate) across all stations in (a) $BATS_{tau\_vis}$ and (b) $BATS_{tau\_NIR}$, as compared to SNOTEL SWE observations. The leftmost column of panels shows a smoothed histogram of the performance metrics across stations. A vertical dashed red line indicates the median metric value, and a horizontal dashed gray line indicates the interquartile range (IQR). The performance metrics are separated by geographic region in the second column; by climate subgroup in the third; and by vegetation type in the fourth. Circles mark the median of the subgroup, and the width of the line marks the interquartile range. If the subgroup has a filled-in circle, it is considered significantly different (p-value < 0.05) from the other subgroups. The number of stations in each subgroup is noted in the legend entries.

References

Abolafia-Rosenzweig, R., He, C., McKenzie Skiles, S., Chen, F., & Gochis, D., 2022: Evaluation and Optimization of Snow Albedo Scheme in Noah-MP Land Surface Model Using In Situ Spectral Observations in the Colorado Rockies. Journal of Advances in Modeling Earth Systems, 14(10), https://doi.org/10.1029/2022MS003141.

Chakravarti, Laha, and Roy, 1967: Handbook of Methods of Applied Statistics, Volume I, John Wiley and Sons, pp. 392-394.

Chen, F., Janjić, Z., & Mitchell, K., 1997: Impact of Atmospheric Surface-layer Parameterizations in the new Land-surface Scheme of the NCEP Mesoscale Eta Model. Boundary-Layer Meteorology, 85(3), 391–421, https://doi.org/10.1023/A:1000531001463.

Currier, W. R., Thorson, T., & Lundquist, J. D., 2017: Independent Evaluation of Frozen Precipitation from WRF and PRISM in the Olympic Mountains. Journal of Hydrometeorology, 18(10), 2681–2703, https://doi.org/10.1175/JHM-D-17-0026.1.

Dickinson, R. E., Henderson-Sellers, A., & Kennedy, P. J., 1986: Biosphere-atmosphere transfer scheme (BATS) for the NCAR community climate model (NCAR Tech. Note NCAR/TN-38+STR, Vol. 82). National Center for Atmospheric Research.

Dickinson, R. E., Shaikh, M., Bryant, R., & Graumlich, L., 1998: Interactive Canopies for a Climate Model. Journal of Climate, 11(11), 2823–2836, https://doi.org/10.1175/1520-0442(1998)011<2823:ICFACM>2.0.CO;2.

Gochis, D.J., M. Barlage, A. Dugger, K. FitzGerald, L. Karsten, M. McAllister, J. McCreight, J. Mills, A. RafieeiNasab, L. Read, K. Sampson, D. Yates, W. Yu, 2018: The WRF-Hydro modeling system technical description, (Version 5.0). NCAR Technical Note. Available online at https://ral.ucar.edu/sites/default/files/public/WRF-HydroV5TechnicalDescription.pdf. doi:10.5065/D6J38RBJ.

Harms, D., Weeks, J., Lea, J., 2016: Comparing SNOTEL extended air temperature sensor and equations to an NSIT certified sensor in an environmental chamber. Seattle, WA.

He, C., Valayamkunnath, P., Barlage, M., Chen, F., Gochis, D., Cabell, R., Schneider, T., Rasmussen, R., Niu, G.-Y., Yang, Z.-L., Niyogi, D., & Ek, M., 2023: The Community

Noah-MP Land Surface Modeling System Technical Description Version 5.0, http://dx.doi.org/10.5065/ew8g-yr95.

He, M., Hogue, T. S., Franz, K. J., Margulis, S. A., & Vrugt, J. A., 2011: Characterizing parameter sensitivity and uncertainty for a snow model across hydroclimatic regimes. Advances in Water Resources, 34(1), 114–127, https://doi.org/10.1016/j.advwatres.2010.10.002.

Hill, D. F., N. Bruhis, S. E. Calos, A. Arendt, and J. Beamer, 2015: Spatial and temporal variability of freshwater discharge into the Gulf of Alaska. J. Geophys. Res., 120, 634–646, https://doi.org/10.1002/2014JC010395.

Jordan, R. E., 1991: A one-dimensional temperature model for a snow cover: Technical documentation for SNTHERM, 89. Retrieved from https://erdc-library.erdc.dren.mil/jspui/bitstream/11681/11677/1/SR-91-16.pdf.

Lettenmaier, D. P., Alsdorf, D., Dozier, J., Huffman, G. J., Pan, M., & Wood, E. F., 2015: Inroads of remote sensing into hydrologic science during the WRR era: REMOTE SENSING. Water Resources Research, 51(9), 7309–7342, https://doi.org/10.1002/2015WR017616.

Kirchner, J., 2001: Data Analysis Toolkit #5: Uncertainty Analysis and Error Propagation. Berkeley Seismology Laboratory. University of California. http://seismo.berkeley.edu/~kirchner/eps_120/Toolkits/Toolkit_05.pdf

Letcher, T., Minder, J., and Naple, P., 2022: Understanding and improving snow processes in Noah-MP over the Northeast United States via the New York State Mesonet. Engineer Research and Development Center (U.S.), http://dx.doi.org/10.21079/11681/45060.

Livneh, B., Deems, J. S., Schneider, D., Barsugli, J. J., and Molotch, N. P., 2014: Filling in the gaps: Inferring spatially distributed precipitation from gauge observations over complex terrain. Water Resources Research, 50(11), 8589–8610, https://doi.org/10.1002/2014WR015442.

Livneh, B., T. Bohn, D. Pierce, F. Munoz-Arriola, B. Nijssen, R. Vose, D. Cayan, and L. Brekke , 2015: A spatially comprehensive, hydrometeorological data set for Mexico, the U.S., and Southern Canada 1950–2013. Sci Data, 2150042, https://doi.org/10.1038/sdata.2015.42.

Niu, G.-Y., and Yang, Z.-L., 2006: Effects of frozen soil on snowmelt runoff and soil water storage at a continental scale. Journal of Hydrometeorology, 7(5), 937–952. https://doi.org/10.1175/JHM538.1.

Niu, G.-Y., Z.-L. Yang, K. E. Mitchell, F. Chen, M. B. Ek, M. Barlage, A. Kumar, K. Manning, D. Niyogi, E. Rosero, M. Tewari, and Y. Xia, 2011: The community Noah land surface model with multiparameterization options (Noah-MP): 1. Model description and evaluation with local-scale measurements. J. Geophys. Res., 116(D12). https://doi.org/10.1029/2010JD015139.

National Oceanic and Atmospheric Administration (NOAA), National Weather Service (NWS), Office of Water Prediction (OWP), Silver Spring, MD., Analysis of Record for Calibration Version 1.1 - Sources, Methods, and Verification. Retrieved from https://hydrology.nws.noaa.gov/aorc-historic/Documents/AORC-Version1.1-SourcesMethodsandVerifications.pdf

Oyler, J. W., S. Z. Dobrowski, A. P. Ballantyne, A. E. Klene, and S. W. Running, 2015: Artificial amplification of warming trends across the mountains of the western United

States. Geophysical Research Letters, 42(1), 153-161, https://doi.org/10.1002/2014GL062803.

Park, S., and S. K. Park, 2016: Parameterization of the snow-covered surface albedo in the Noah-MP Version 1.0 by implementing vegetation effects. Geosci. Model Dev., 9(3), 1073–1085. https://doi.org/10.5194/gmd-9-1073-2016.

Sakaguchi, K., and X. Zeng, 2009: Effects of soil wetness, plant litter, and under-canopy atmospheric stability on ground evaporation in the Community Land Model (CLM3.5): New schemes for CLM3.5 soil evaporation. J. Geophys. Res. Atmos., 114(D1). https://doi.org/10.1029/2008JD010834.

Serreze, M. C., Clark, M. P., Armstrong, R. L., McGinnis, D. A., and Pulwarty, R. S., 1999: Characteristics of the western United States snowpack from snowpack telemetry (SNOTEL) data. Water Resources Research, 35(7), 2145–2160, https://doi.org/10.1029/1999WR900090.

Sun, N., Yan, H., Wigmosta, M. S., Leung, L. R., Skaggs, R., and Hou, Z., 2019: Regional Snow Parameters Estimation for Large-Domain Hydrological Applications in the Western United States. Journal of Geophysical Research: Atmospheres, 124(10), 5296–5313. https://doi.org/10.1029/2018JD030140.

Vose, R.S., and Coauthors, 2014: Improved historical temperature and precipitation time series for US climate divisions. J. Appl. Meteor. Climatol., 53, 1232-1251, https://doi.org/10.1175/JAMC-D-13-0248.1

Wang, Y., Broxton, P., Fang, Y., Behrangi, A., Barlage, M., Zeng, X., & Niu, G., 2019: A Wet-Bulb Temperature-Based Rain-Snow Partitioning Scheme Improves Snowpack Prediction

Over the Drier Western United States. Geophysical Research Letters, 46(23), 13825–13835, https://doi.org/10.1029/2019GL085722.

Wiken, E., Jiménez Nava, F., and Griffith, G., 2011: North American Terrestrial Ecoregions—Level III. Commission for Environmental Cooperation, Montreal, Canada.

Yan H., N. Sun, M. Wigmosta, R. Skaggs, Z. Hou, and R. Leung, 2018: Next-generation intensity-duration-frequency curves for hydrologic design in snow-dominated environments. Water Resources Research, 54(2), 1093–1108, https://doi.org/10.1002/2017WR021290.

Yang, Z.-L., and Dickinson, R. E., 1996: Description of the Biosphere-Atmosphere Transfer Scheme (BATS) for the soil moisture workshop and evaluation of its performance. Global Planet. Change, 13, 117–134, https://doi.org/10.1016/0921-8181(95)00041-0.

Zhang, G., Zhou, G., Chen, F., Barlage, M., & Xue, L., 2014: A Trial to Improve Surface Heat Exchange Simulation through Sensitivity Experiments over a Desert Steppe Site. Journal of Hydrometeorology, 15, 664-684, https://doi.org/10.1175/JHM-D-13-0113.1.